Bias Smith Tube Optimization of Drain Voltage and Load Reflection Coefficient to Maximize Power-Added Efficiency Under ACPR Constraints for Radar Power Amplifiers

MATTHEW FELLOWS, Student Member, IEEE
Sandia National Laboratories, Livermore, CA USA

SARVIN REZAYAT, Student Member, IEEE
National Instruments, Austin, TX USA

LUCILIA LAMERS, Student Member, IEEE
Oncor, Dallas, TX USA

JOSEPH BARKATE, Student Member, IEEE
ALEXANDER TSATSOULAS, Student Member, IEEE
Baylor University, Waco, TX USA

CHARLES BAYLIS, Senior Member, IEEE
Baylor University, Waco, TX USA

LAWRENCE COHEN, Senior Member, IEEE
Naval Research Laboratory, Washington, DC USA

ROBERT J. MARKS II, Fellow, IEEE, Fellow, OSA
Baylor University, Waco, TX USA

Manuscript received July 5, 2016; revised May 10, 2017 and July 3, 2017; released for publication August 23, 2017. Date of publication July 13, 2018; date of current version February 7, 2019.

DOI. No. 10.1109/TAES.2018.2849239

Refereeing of this contribution was handled by R. Adve.

This work was supported by the National Science Foundation under Grant ECCS-1343316.

Author's addresses: M. Fellows was with Baylor University, Waco, TX 76706, USA. He is now with the Sandia National Laboratories, Livermore, CA 94550, USA, E-mail: (docfellows@gmail.com). S. Rezayat was with Baylor University, Waco, TX 76706, USA. She is now with National Instruments, Austin, TX 78759, USA, E-mail: (Sarvin_Rezayat@alumni.baylor.edu). L. Lamers was with Baylor University, Waco, TX 76706, USA. She is now with Oncor, Dallas, TX 75202, USA, E-mail: (Luci_Lamers@alumni.baylor.edu). J. Barkate and A. Tsatsoulas were with Baylor University, Waco, TX 76706, USA, E-mail: (Joseph_Barkate@alumni.baylor.edu; Alexander_Tsatsoulas@baylor.edu). C. Baylis and R. J. Marks II are with Baylor University, Waco, TX 76706, USA, E-mail: (Charles_Baylis@baylor.edu; Robert_Marks@baylor.edu). L. Cohen is with the Naval Research Laboratory, Washington, DC 20375, USA, E-mail: (lawrence.cohen@nrl.navy.mil). *(Corresponding author: Charles Baylis.)*

Reconfigurable transmitter power amplifiers will be necessary in future cognitive radar systems to allow adjustment in operating frequency, spectral output, and other desired operating characteristics while maintaining performance. Circuit optimization algorithms for tuning the amplifier load impedance and bias voltage in real time should maximize power-added efficiency while limiting the adjacent-channel power ratio (ACPR) in order to obtain spectral compliance. This paper presents a fast vector-based three-dimensional optimization for simultaneous bias adjustment and impedance matching for these goals using the bias Smith tube as the optimization space. Simulation and measurement results are presented for this optimization algorithm, and correspondence between the results is examined for several different starting locations in the bias Smith tube. This algorithm will allow simultaneous optimization of bias voltage and load impedance in real time in order to meet changing requirements.

I. INTRODUCTION

Future adaptive radar transmitters will need the ability to dynamically reconfigure in order to share the frequency spectrum more effectively without sacrificing transmitter power efficiency. The concept of adaptive radar has existed for several decades [1]–[4], but more recent work shows that adaptive radar technology is moving from theory to reality. A similar technology called cognitive radar has also been proposed. While adaptive radar systems adjust designs in real time for changing requirements, cognitive radar systems additionally learn from and respond to their environment [5], [6].

The use of adaptive and cognitive radars in sharing of the frequency spectrum in real time is a significantly challenging effort. Collaborative efforts between radar and communications using cognitive radio technology are beginning to emerge [7]. A recent paper discusses the concept of joint circuit and waveform codesign as a significant challenge problem facing radar operators [8]. This allows the intertwined impact of the circuit and the waveform to be jointly considered. Circuit optimizations and waveform optimizations should be designed to operate simultaneously in real time. Patton demonstrates the joint optimization of the waveform and receiver's matched filtering for autocorrelation and cross-correlation constraints [9], synthesis of a waveform based on a desired spectrum [10], and waveform optimization to meet constraints on both the autocorrelation and the waveform amplitude [11]. Jakabosky describes optimization of radar waveforms with the transmitter hardware "in the loop" to overcome the tradeoff of distortion versus transmission efficiency [12], and Ryan and Blunt demonstrate the hardware-in-the-loop optimization of polyphase-coded frequency-modulation waveforms using a linear amplification with nonlinear components power-amplifier architecture [13], [14]. Techniques for real-time circuit optimization that can be used in conjunction with waveform optimization techniques have also been recently introduced to the radar community. Real-time optimization of load impedance in a radar transmitter will require a variable matching circuit [15], [16]. Kingsley and Guerci have discussed implementation of a matching network for adaptive radar [15]. The literature shows that tuning of some matching circuits can be achieved in microseconds, which is fast enough for real-time optimization purposes. Previous works by the authors have presented algorithms for fast circuit tuning, including the ability to tune the load reflection coefficient presented to an amplifier to maximize the power-added efficiency (PAE) under constraints on the adjacent-channel power ratio (ACPR), using the Smith chart as a search space [17], [18]. ACPR and PAE are both significantly dependent on load impedance [19]. Instead of the ACPR, the circuit optimization can be performed specifically to require spectral mask compliance [20]. Our development of the Smith tube, a multidimensional optimization space, has allowed additional parameters to be modified in the optimization, including waveform bandwidth [21] and input power [22]. In addition, the optimization can include additional constraints, such as requiring the output power to be above a specified minimum value [23].

The purpose of this paper is to demonstrate a joint optimization of the power-amplifier matching circuit impedance and an amplifier device bias voltage to maximize the efficiency of the amplifier while remaining within constraints on the ACPR. Our work builds on the following previous innovations from the literature: 1) PAE and ACPR dependence on load impedance and bias and 2) fast algorithms for circuit optimization. The need for joint circuit and bias optimization is developed by several works that show the dependence of PAE and ACPR on bias voltage and impedance. This literature includes applications such as envelope modulation of gate voltage [24], adjusting drain voltage and current to improve PAE [25], variation of input and output bias voltages [26], optimizing bias and RF power for efficiency while examining drain voltage and RF input [27], and using a dc–dc converter to simultaneously optimize input waveform and dc voltage [28]. Other literature shows how load resistance impacts bias point and power efficiency [29], how the optimum load impedances for power and efficiency vary with bias voltage on the Smith chart [30], how optimum PAE varies with bias [31], and how to select matching circuit impedance and bias voltage for ideal peaking and carrier performance using Doherty amplifiers [32]. Recent work by the authors has introduced the bias Smith tube, which is a three-dimensional extension of the Smith chart where the vertical dimension is drain voltage [33]. The bias Smith tube is shown in Fig. 1.

Several circuit optimization techniques have been developed in the literature. Sun and Lau implement a genetic algorithm for antenna matching based on VSWR requirements [34], [35]. Qiao also uses a genetic algorithm for a reconfigurable amplifier [36]. However, genetic algorithms can be slower than other algorithm types for certain impedance-matching applications [37]. Balachandran demonstrates the application of the sequential unconstrained minimization technique and the automated Lagrangian penalty function technique in designing a power converter [38]. The constrained optimization for PAE while meeting ACPR requirements is an example of an optimization involving more than one objective. The literature describes several methods for optimizing in multi-objective situations [39]–[44].

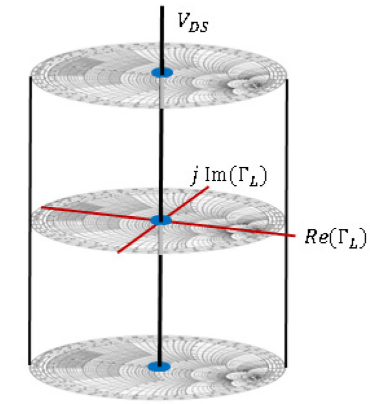

Fig. 1. Bias Smith tube. The vertical axis represents a bias voltage (drain–source voltage V_{DS} in this case), while the horizontal cross section of the tube is a conventional Smith chart [33].

The rest of this paper describes the presented algorithm and shows simulation and measurement results of algorithm testing. Section II describes the bias Smith tube search algorithm in detail. Section III shows simulation results for this algorithm. Section IV shows measurement results for this algorithm. Section V provides some conclusions and suggestions for future work.

II. ALGORITHM DESCRIPTION

The presented algorithm simultaneously optimizes the load reflection coefficient Γ_L with a device bias voltage in the bias Smith tube. It starts from a user-specified location in the bias Smith tube and uses a vector-based approach to find the maximum PAE value that can be obtained within a user-defined ACPR limit. In addition to the ACPR limit, the algorithm requires a few other user inputs. The user must provide the value for the step size parameter D_s, which is used in calculating the magnitudes of all steps the search will take. Additionally, the user must define the resolution distance D_r, as well as the neighboring-point distance D_n used for estimating the gradient near a candidate point. When the magnitude of the search vector decreases below D_r, the search is stopped. Third, the user must provide minimum and maximum drain voltages to be considered by the algorithm. Finally, the user must provide the values of Γ_L and voltage V_{DS} to serve as the start location for the algorithm in the Smith tube. The input parameters and their descriptions are summarized in Table I.

Once those inputs have been defined, the V_{DS} values are normalized between -1 and 1 using the following equation:

$$v_{\mathrm{DS}} = 2\frac{V_{\mathrm{DS}} - V_{\mathrm{DS,\,min}}}{V_{\mathrm{DS,\,max}} - V_{\mathrm{ds,\,min}}} - 1 \tag{1}$$

where v_{DS} is the normalized drain voltage, V_{DS} is the drain voltage, $V_{\mathrm{DS,\,min}}$ is the minimum drain voltage to be considered by the algorithm, and $V_{\mathrm{DS,\,max}}$ is the maximum drain voltage to be considered by the algorithm. Normalizing the V_{DS} values establishes the top and bottom of the Smith tube while also causing the vertical dimension of the Smith tube to have the same scale (going from -1 to 1) as the

TABLE I
Algorithm Input Parameters

Parameter	Description
$ACPR_{limit}$	Maximum ACPR constraint
D_s	Search distance parameter
D_n	Neighboring-point distance parameter for gradient estimation
D_r	Resolution distance parameter for search termination
$V_{DS,max}$	Maximum allowable value of V_{DS} (V)
$V_{DS,min}$	Minimum allowable value of V_{DS} (V)
$\Gamma_{L,start}$	Starting load reflection coefficient for the search
$V_{DS,start}$	Starting drain-source voltage for the search

horizontal dimension (load reflection coefficient Γ_L on the Smith chart), which is normalized according to the well-known equation $z_L = Z_L/Z_0$, where z_L is the normalized load impedance, Z_L is the load impedance, and Z_0 is the reference impedance.

A flowchart describing the basic progression of the algorithm is shown in Fig. 2. After the algorithm normalizes the V_{DS} values, it starts taking measurements at the user-specified start location. The algorithm takes a measurement at that candidate location and at three neighboring points separated from the initial point by neighboring-point distance D_n in each dimension of the search, as shown in Fig. 3. These measurements are then used to estimate gradients in order to determine the direction of steepest descent for the ACPR (represented in equations by $\hat{a}$) and the direction of steepest ascent for PAE (represented in equations by $\hat{p}$). Based on those measurements, the search will then calculate a step vector, which depends on where the candidate lies in the Smith tube.

Unit vectors $\hat{a}$ and $\hat{p}$ are estimated in the optimal PAE and ACPR, based on the approximations of the gradients. If the PAE is represented by p, then the PAE gradient is given by ∇p:

$$\nabla p = \hat{\Gamma}_r \frac{\partial p}{\partial \Gamma_r} + \hat{\Gamma}_i \frac{\partial p}{\partial \Gamma_i} + \hat{v}_{\text{DS}} \frac{\partial p}{\partial v_{\text{DS}}}. \tag{2}$$

The partial derivatives in (2) are approximated as follows, where Δp in each case represents the change in p when the associated step is taken in the bias Smith tube:

$$\frac{\partial p}{\partial \Gamma_r} \approx \frac{\Delta p}{\Delta \Gamma_r} = \frac{\Delta p}{D_n}. \tag{3}$$

$$\frac{\partial p}{\partial \Gamma_i} \approx \frac{\Delta p}{\Delta \Gamma_i} = \frac{\Delta p}{D_n}. \tag{4}$$

$$\frac{\partial p}{\partial v_{\text{DS}}} \approx \frac{\Delta p}{\Delta v_{\text{DS}}} = \frac{\Delta p}{D_n}. \tag{5}$$

The unit vector in the direction of PAE steepest ascent is calculated using a gradient estimation:

$$\hat{p} = \frac{\nabla p}{|\nabla p|}. \tag{6}$$

The ACPR gradient ∇a, where a is used to represent the ACPR, is estimated using the same approach as outlined in

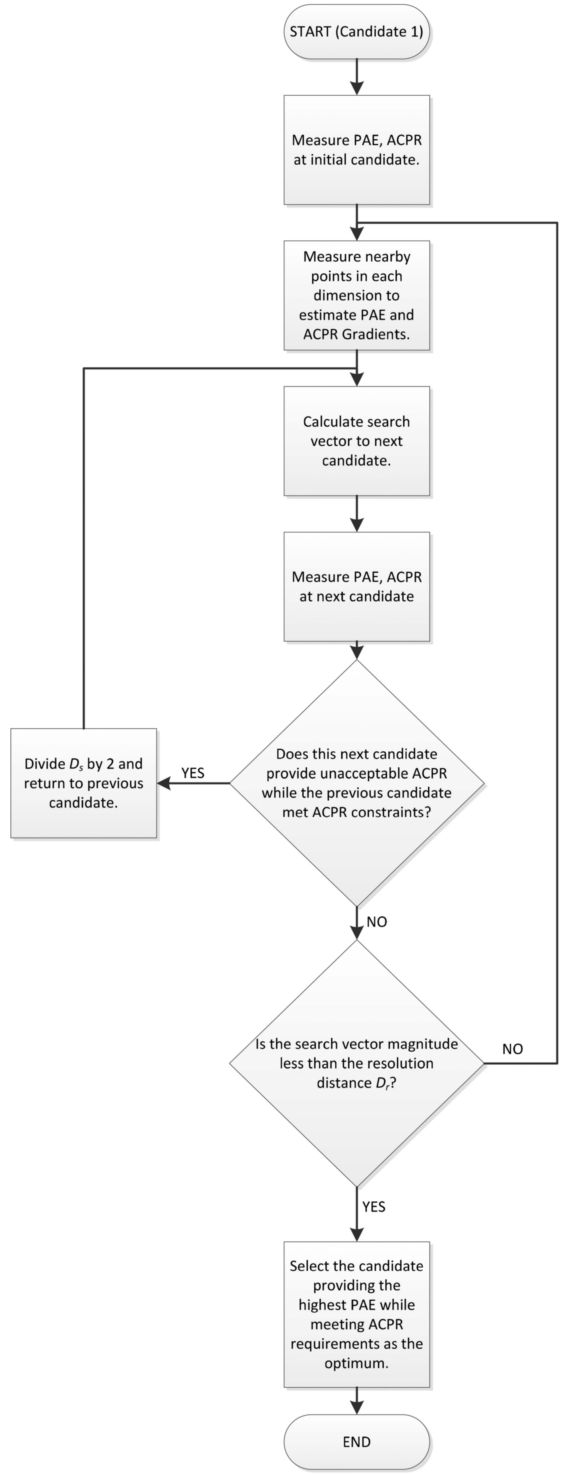

Fig. 2. Bias Smith tube search algorithm flowchart.

(2)–(6), with a replacing p. A unit vector $\hat{a}$ is defined in the optimal direction of ACPR travel, which is opposite to the gradient, because the ACPR improves as it grows smaller. Thus, $\hat{a}$ is given in the direction of ACPR steepest descent:

$$\hat{a} = -\frac{\nabla a}{|\nabla a|}. \tag{7}$$

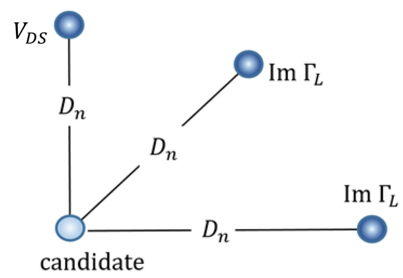

Fig. 3. Measured Γ_L points for PAE and ACPR gradient estimation at a candidate. Points are measured separated from the candidate by neighboring-point distance D_n in all three coordinate directions.

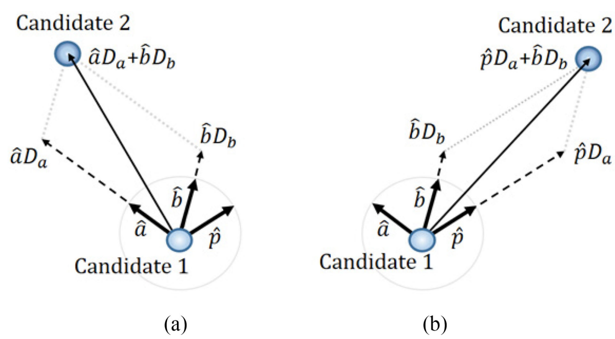

Fig. 4. Search vectors in the Smith tube in the cases where (a) candidate 1 ACPR is outside the ACPR limit and (b) candidate 1 ACPR is inside the ACPR limit.

A unit vector $\hat{b}$ bisecting $\hat{a}$ and $\hat{p}$ is estimated:

$$\hat{b} = \frac{1}{2}\left(\hat{a} + \hat{p}\right). \tag{8}$$

If the measurement at the current candidate location gives an ACPR that was greater than the ACPR limit (out of compliance), then the step vector is defined by

$$\bar{v} = \hat{a}\ D_a + \hat{b}D_b \tag{9}$$

where

$$D_a = \frac{D_s}{2}\frac{|\mathrm{ACPR_{cand}} - \mathrm{ACPR_{limit}}|}{|\mathrm{ACPR_{worst}} - \mathrm{ACPR_{limit}}|}, \tag{10}$$

$$D_b = \frac{D_s}{2}\frac{|\theta - 90^\circ|}{90^\circ}. \tag{11}$$

This search vector construction is shown in Fig. 4(a). $\mathrm{ACPR_{cand}}$ is the measured ACPR at the candidate location, $\mathrm{ACPR_{limit}}$ is the user-defined ACPR limit, and $\mathrm{ACPR_{worst}}$ is the measured ACPR value that is farthest from the ACPR limit. Note that $D_a = 0$ if the ACPR at the candidate is equal to the ACPR limit. In (13), θ is the value of the bisector angle between $\hat{a}$ and $\hat{p}$. Note that $D_b = 0$ if the bisector angle is equal to 90°. If $\theta = 90^\circ$, the ACPR and PAE contours are collinear, which means that any location with $\theta = 90^\circ$ will have the maximum PAE value for some ACPR limit (assuming convex contours). The collection of all points with $\theta = 90^\circ$ forms the Pareto optimum locus [17].

The ACPR contours may not always be convex; however, the authors have observed that the ACPR contours are usually close enough to being convex in the regions near the desired optimum for the search algorithm to provide a consistent quality of results for all start locations in the Smith tube. Since (3) goes to zero on the ACPR limit contour and (4) goes to zero on the Pareto front, the vector addition in (2) should converge to the desired optimum.

A second possibility based on a candidate measurement is that the ACPR at the candidate will be less than or equal to the ACPR limit, which means that the present candidate is in spectral compliance. In that case, the next step, which the algorithm takes, is defined by

$$\bar{v} = \hat{p}\ D_a + \hat{b}D_b. \tag{12}$$

The only difference between (12) and (9) is that the vector in (12) has a component in the direction of steepest ascent for PAE, whereas the vector in (9) has a component in the direction of steepest descent for the ACPR. This difference recognizes which of those two parameters needs improvement. If the ACPR limit is being met then the algorithm tries to improve PAE. If the ACPR limit is not being met then the algorithm tries to improve the ACPR. Also note that D_a and D_b in (12) are the same as in (9), which means that (12) and (9) will both converge to the desired optimum location. Fig. 4(b) shows a representation of the step the search will take in this case.

Before the algorithm can use the calculated step vector, it must first check to make sure that the new candidate location is still inside the Smith tube. If not, the algorithm chooses the closest location to the calculated point that is inside the Smith tube to be the next candidate point. The algorithm then moves to take a measurement at the new location and performs the following checks.

1) The step to a new candidate point is allowed to leave the ACPR acceptable region one time. After the first time, if the step took the search from a candidate inside the ACPR acceptable region to a candidate outside the ACPR acceptable region, divide the search distance parameter D_s by 2 and recalculate the step. This forces the algorithm to converge to an optimum even if the user-chosen D_s value is too large for (9) and (12) to decrease naturally below the resolution distance D_r.
2) If both the new candidate and the old candidate are inside the ACPR acceptable region, but the PAE at the new candidate is lower (worse) than the PAE at the old candidate, divide D_s by 2 and recalculate the step. This allows the algorithm to still converge to the constrained optimum in the case where the global PAE maximum is inside the ACPR acceptable region.

The presented search algorithm repeats the process of candidate measurements and steps to new candidates until the magnitude of the step vector $\bar{v}$ is less than the user-defined resolution distance D_r. When that happens, the algorithm takes its last candidate measurement and then chooses the measured point with the maximum PAE within the ACPR limit as the optimum point. This point is the combination of bias voltage and Γ_L that provides the constrained optimum PAE.

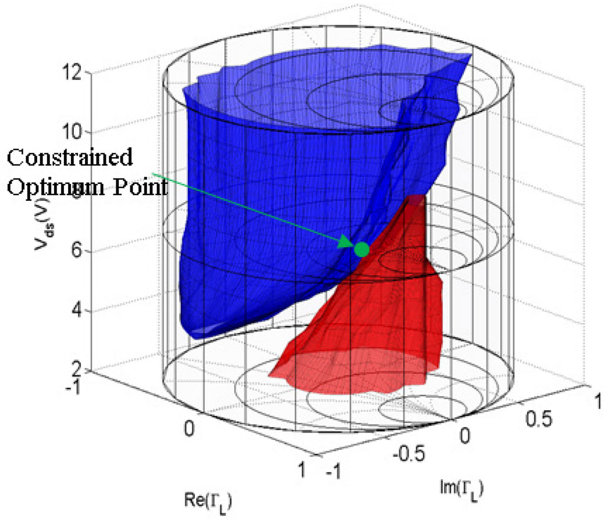

Fig. 5. Surface for ACPR $= -49$ dBc (blue) and surface with PAE $=$ 33.04% (red) from simulations. The constrained optimum point is $\Gamma_L =$ 0.2/90°, $V_{\mathrm{DS}} = 6$ V.

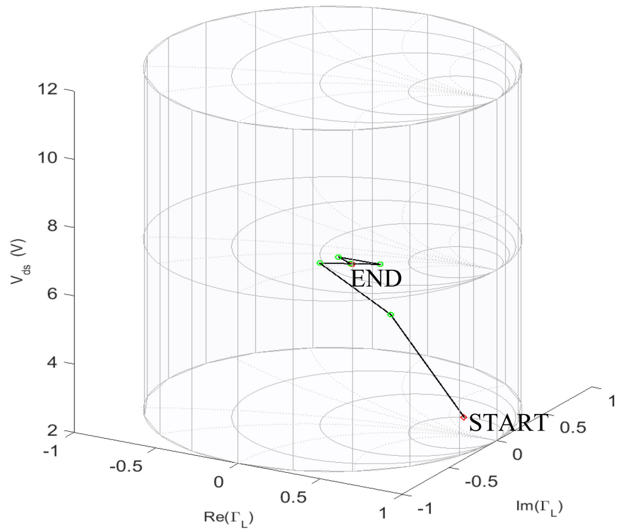

Fig. 6. Simulation search trajectory for starting $\Gamma_L = 0.8/0°$ with V_{DS} $= 2.5$ V. The search converges to a constrained optimum at $\Gamma_L =$ 0.17/83° with $V_{\mathrm{DS}} = 6.02$ V, requiring a total of 26 measurements. The constrained optimum PAE is 33.12%, with final ACPR $= -49.06$ dBc.

III. SIMULATION RESULTS

The presented algorithm was tested in simulation using the Advanced Design System (ADS) software from Keysight Technologies. In ADS, a Modelithics model of a Qorvo TGF2960 field-effect transistor was used. The search used an ACPR limit of -49 dBc and was tested from a total of 50 different start locations in the Smith tube. Simulations were performed using a CDMA2000 excitation waveform at a fixed center frequency of 3.3 GHz, input power $P_{\mathrm{in}} = 9$ dBm, and gate voltage $V_{\mathrm{GS}} = 0.9$ V. The drain voltage V_{DS} was allowed to vary between 2 and 12 V.

Fig. 5 shows the surface representing ACPR $= -49$ dBc and the surface representing PAE $= 33.04\%$, which represents the largest PAE value that can be obtained within that ACPR limit. The point where the two surfaces intersect in that figure represents the optimum operating point as found by a brute force examination of the entire Smith tube, which requires hundreds of simulated points, taken by multiple load-pull simulations at varying V_{DS} values. The goal of the presented optimization algorithm is to avoid the necessity for this exhaustive measurement performance and find the optimum operating point as quickly as possible.

Figs. 6 and 7 show examples for the search trajectories of the fast search algorithm from two different starting locations. These results are typical examples of the path that the algorithm will take to reach the optimum. Table II shows data for a few selected algorithm runs for various starting points throughout the V_{DS} Smith tube, and Table III shows statistics summarizing the algorithm results for 50 different simulation start locations. Table II shows some variation in the final V_{DS} values obtained by the algorithm. While, on first thought, this may appear to be contrary to expectations, such differences in the end V_{DS} value may be expected to occur, since the ACPR and PAE surfaces in Fig. 5 are very close together for a wide range of V_{DS}.

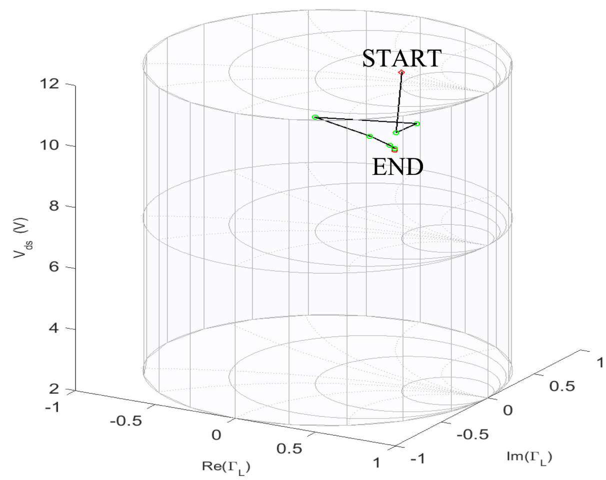

Fig. 7. Simulation search trajectory for starting $\Gamma_L = 0.8/90°$ with V_{DS}= 10.5 V. The search converges to a constrained optimum at $\Gamma_L =$ 0.38/49° with $V_{\mathrm{DS}} = 9.01$ V, requiring a total of 31 measurements. The constrained optimum PAE is 31.92%, with final ACPR $= -49.14$ dBc.

What is important is that these results show similarity in the constrained optimum PAE values.

Tables II and III also show an additional significant result of the algorithm: its effect on the output power P_d delivered by the amplifier. In practice, maintaining sufficient output power is important to successfully illuminate and receive information from radar targets. Since the output power is not included as a constraint, it can potentially be affected by the optimization, as both P_d and V_{DS} play an important role in determining the PAE, which is given by the following equation:

$$\mathrm{PAE} = \frac{P_d - P_{\mathrm{in}}}{V_{\mathrm{DS}} I_D} \times 100\%. \tag{13}$$

Thus, the PAE can be increased by either increasing the output power P_d or decreasing the drain–source voltage

TABLE II
Simulation Results for Different Starting Points

Start Γ_L	Start V_{DS} (V)	End Γ_L	End V_{DS} (V)	End ACPR (dBc)	End PAE (%)	End P_d (dBm)	Gain (dB)	# Meas
0	2.5	$0.14\underline{/144^\circ}$	5.01	-49.05	32.05	21.69	12.69	22
$0.8\underline{/0^\circ}$	4.5	$0.19\underline{/69^\circ}$	6.45	-49.43	32.90	23.12	14.12	27
$0.8\underline{/90^\circ}$	6.5	$0.23\underline{/74^\circ}$	6.57	-49.07	33.15	23.23	14.23	31
$0.8\underline{/180^\circ}$	8.5	$0.18\underline{/60^\circ}$	6.52	-49.29	32.86	23.17	14.17	31
$0.8\underline{/-90^\circ}$	10.5	$0.34\underline{/52^\circ}$	8.19	-49.12	32.45	24.32	15.32	38

TABLE III
Summary of Results for All Simulated Start Locations

	Average	Median	Standard Deviation
End ACPR	-49.26 dBc	-49.19 dBc	0.22 dBc
End PAE	32.49%	32.62%	0.52%
End P_d	23.34 dBm	23.15 dBm	1.00 dBm
Mean # of Measurements	32.1	31.0	8.8
End V_{DS}	6.92 V	6.49 V	1.38 V

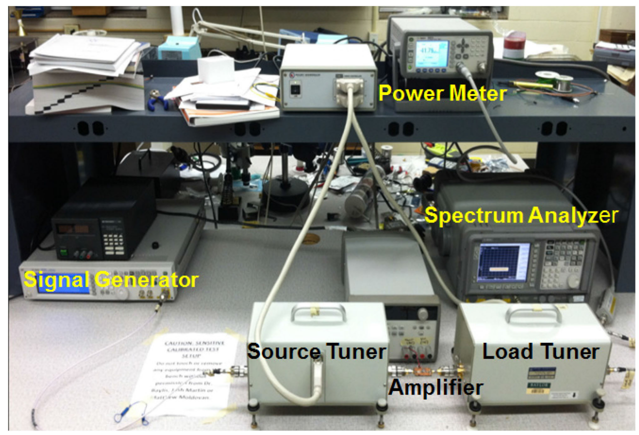

Fig. 8. Measurement test setup.

$V_{\rm DS}$. The associated gain is also shown in Table II. It can be seen that the gain and P_d are significantly lower for the starting point $\Gamma_L = 0$, $V_{\rm DS} = 2.5$ V than for many of the other starting points. For this starting point, the end $V_{\rm DS}$ value is also lower. The lowering of both P_d and $V_{\rm DS}$ causes the PAE to be approximately the same as for the other starting points. An opposite effect is seen for the starting point $\Gamma_L = 0.8/{-90^\circ}$, $V_{\rm DS} = 10.5$ V, where the values of P_d and gain are approximately 1 dB higher than for the other starting points. However, the end value of $V_{\rm DS}$ is over 1.5 V greater than any of the other points shown in the table. While the higher value of P_d increases the PAE, the higher value of $V_{\rm DS}$ lowers it so that the PAE value is approximately the same as the other endpoints displayed in the table. As such, there is some variation in the output power values. The standard deviation of the end P_d values is shown in Table III to be 1 dBm, which is significant; however, the PAE value standard deviation is only 0.52%. Whether these variations are acceptable in practice depends on the system-level specifications regarding target illumination power and expected path loss. This is an important topic for future work.

IV. MEASUREMENT RESULTS

In addition to the simulated algorithm runs in ADS, the presented algorithm was tested in measurement for 20 different starting points using a Maury Microwave Automated Tuner System. Fig. 8 shows the measurement setup for bench testing. The load impedance tuner provides the desired Γ_L. A power meter is used for the PAE measurements, and a spectrum analyzer is used to measure the ACPR. The desired waveform is produced by a signal generator. A Microwave Technology MWT-173 GaAs metal–semiconductor field-effect transistor was used for the measurement testing of the algorithm. This is a different device than was used for the simulations, in an effort to provide a different scenario to test algorithm operation. The waveform used for these measurement tests was a modified chirp waveform centered at 3.3 GHz. This waveform consisted of a constant tone as well as a tone that sweeps in frequency, and the bandwidth of the waveform was 16 MHz. The input power to the amplifier was held constant at 14.5 dBm, the gate voltage $V_{\rm GS}$ was held constant at -1.5 V, and $V_{\rm DS}$ was allowed to vary from 2 to 6 V. An ACPR limit of -28.5 dBc was used for the measurement testing.

Fig. 9 shows the surface representing ACPR $= -28.5$ dBc and the surface representing PAE $= 32.19\%$, which represents the largest PAE value that can be obtained within the ACPR limit. The point where the two surfaces intersect in that figure represents the constrained optimum combination of Γ_L and $V_{\rm DS}$ as found by a brute force examination of the entire Smith tube, which requires hundreds

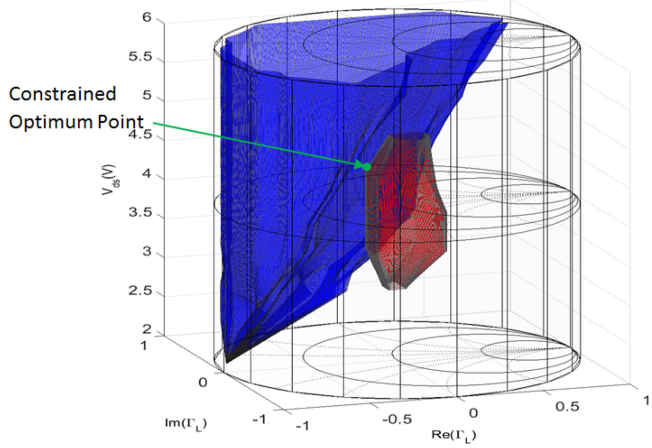

Fig. 9. Acceptable region for the ACPR limit of −28.5 dBc and region with the PAE greater than 32.49%, taken from traditional load-pull measurements at multiple values of V_{DS}. The constrained optimum is found at $\Gamma_L = 0.22/158°$ and $V_{DS} = 4.5$ V.

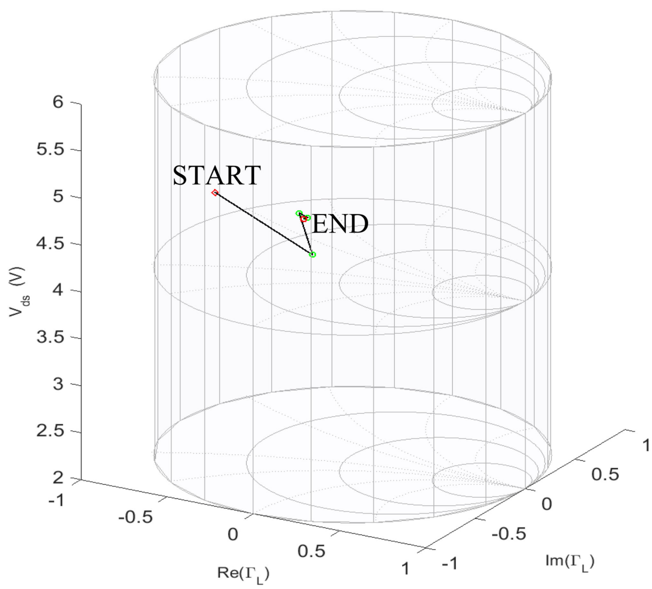

Fig. 10. Measurement search trajectory for starting $\Gamma_L = 0.8/180°$ with $V_{DS} = 4.5$ V. The search converges to a constrained optimum at $\Gamma_L = 0.25/-141°$, $V_{DS} = 4.54$ V, requiring a total of 24 measurements. The constrained optimum PAE is 34.35%, with final ACPR = −28.65 dBc.

of measured points. Also note that, similar to the device used for simulation, the PAE and ACPR surfaces are close together for a large V_{DS} range, which could result in a fairly large range of final V_{DS} values for the constrained optima found by different algorithm runs.

Figs. 10 and 11 show the results of running the search algorithm from two different Smith tube starting locations. Table IV shows data for a few selected algorithm runs for various starting points throughout the Smith tube, and Table V shows statistics summarizing the algorithm's results for all 20 start locations that were measured.

For the most part, the results in Tables IV and V show consistent PAE results with some variation in the end locations due to the large region where the PAE and ACPR contours are close together, much like in simulation.

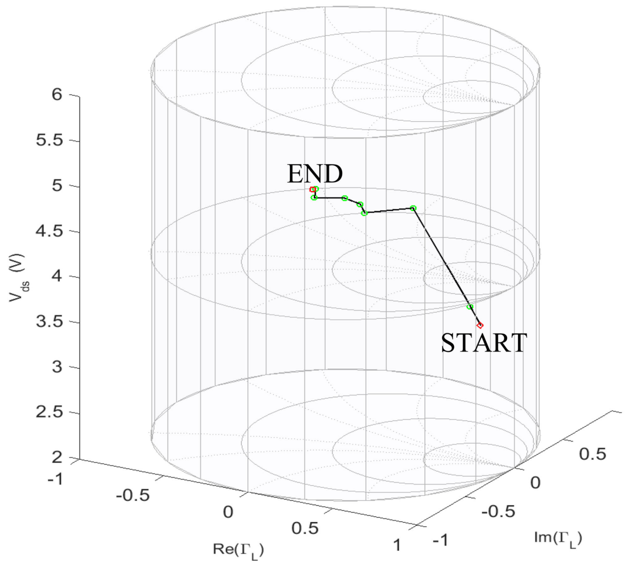

Fig. 11. Measurement search trajectory for starting $\Gamma_L = 0.8/0°$ with $V_{DS} = 3.5$ V. The search converges to a constrained optimum at $\Gamma_L = 0.35/149°$, V_{DS}= 4.48 V, requiring a total of 32 measurements. The constrained optimum PAE is 30.62%, with final ACPR = −28.75 dBc.

TABLE IV
Measurement Results for Different Starting Points

Start Γ_L	Start V_{DS} (V)	End Γ_L	End V_{DS} (V)	End ACPR (dBc)	End PAE (%)	# Meas
0.8/0°	2.5	0.45/170°	4.18	-28.63	30.05	50
0.8/0°	4.5	0.24/-132°	4.48	-28.75	30.62	41
0.8/90°	3.5	0.39/157°	4.37	-28.69	30.70	31
0.8/90°	5.5	0.28/-128°	4.86	-28.70	33.92	30
0.8/180°	2.5	0.58/177°	3.81	-28.62	24.98	44
0.8/180°	4.5	0.25/-141°	4.54	-28.65	34.35	24
0.8/-90°	3.5	0.25/-133°	4.68	-28.61	34.42	40
0.8/-90°	5.5	0.28/-129°	5.18	-28.99	32.61	24
0	2.5	0.40/-163°	4.90	-28.60	34.75	73
0	4.5	0.23/-132°	2.90	-28.52	34.12	39

TABLE V
Summary of Results for All Measured Start Locations

	Average	Median	Standard Deviation
End ACPR	-28.69 dBc	28.66 dBc	0.113 dBc
End PAE	32.35%	33.74%	2.64%
# of Measurements	36.1	35.5	12.4
End V_{DS}	4.67 V	4.69 V	0.44 V

However, the start location at $\Gamma_L = 0.8/180^\circ$ and $V_{DS} = 2.5$ V showed a lower quality result. Further analysis of the Smith tube in this region revealed that the ACPR contours in that area are very flat and not convex, which causes the algorithm to divide its step size down and stop the search too early. This type of ACPR contour is a common occurrence for start locations, which are particularly far from the desired optimum for the search algorithm. This demonstrates the importance of either choosing start locations that are close to the desired optimum or carefully selecting the boundaries of the Smith tube such that regions that are far from the desired optimum are not considered by the search algorithm.

While the adjustment of drain bias voltage has been specifically examined in this paper, it is also possible to consider the real time, simultaneous optimization of the gate–drain voltage bias V_{GS}. Adjusting V_{GS} would essentially allow the operating class of the amplifier to vary between classes A, AB, B, and C. This would allow further exploitation of the tradeoff between linearity and efficiency. Class A, one extreme, would provide excellent ACPR but would lower PAE, while class C is most likely to provide very high PAE while resulting in a much higher ACPR. The real-time optimization for amplifier class could allow the amplifier to make real-time transitions between the classes based on waveform changes as well. If a larger amplitude message were to be provided, the amplifier could raise its V_{GS} automatically by rerunning the optimization. This would preserve linearity. However, if a small amplitude signal is then provided to the amplifier, the optimization could be rerun and would likely result in a lower value of V_{GS}, preserving efficiency. As such, real-time optimizations of either (or potentially both) bias voltages of a transistor should be very useful.

This work represents an initial algorithm for the optimization of PAE and ACPR by simultaneous optimization of load impedance and bias voltage. As discussed earlier, in a practical radar system, output power and gain will also be important criteria of the radar transmitter amplifier. It is critical for the transmitted power of the radar to be sufficient to illuminate the target such that a reflection can be detected above the noise floor at the receiver. Such considerations could be used to derive a minimum output power of the transmitter and its power amplifier. This improvement of the search would include the minimum amplifier output power as an additional constraint in the bias Smith tube search, in a similar approach to that recently demonstrated in the Smith chart [23].

V. CONCLUSION

A fast search algorithm has been presented to find the combination of load reflection coefficient and drain voltage in the V_{DS} Smith tube to maximize PAE within an ACPR constraint. This is the first demonstration of simulation- and measurement-based joint matching circuit and bias voltage optimization using the Smith tube framework. Simulation and measurement results for the algorithm have been shown to demonstrate the effectiveness of the algorithm under a variety of conditions. A potential weakness of the algorithm when using start locations far from the desired optimum has also been demonstrated, and possible methods for avoiding this weakness have been suggested. This algorithm is expected to find usefulness in future adaptive radar transmitters, which need to adjust their operating parameters to changing requirements in real time.

ACKNOWLEDGMENT

The authors wish to thank Keysight Technologies for cost-free loan of the Advanced Design System software, and Modelithics for donation of model libraries through the Modelithics University Program. The authors are grateful to D. Macias of Baylor University for data collection during the revisions of this paper.

REFERENCES

[1] L. E. Brennan and I. S. Reed
Theory of adaptive radar
IEEE Trans. Aerosp. Electron. Syst., vol. 9, no. 2, pp. 237–252, Mar. 1973.

[2] D. T. Gjessing, J. Hjelmstad, and T. Lund
A multifrequency adaptive radar for detection and identification of objects: Results on preliminary experiments on aircraft against a sea-clutter background
IEEE Trans. Aerosp. Propag., vol. AP-30, no. 3, pp. 351–365, May 1982.

[3] J. S. Goldstein and I. S. Reed
Theory of partially adaptive radar
IEEE Trans. Aerosp. Electron. Syst., vol. 33, no. 4, pp. 1309–1325, Oct. 1997.

[4] *Adaptive Radar Signal Processing*, S. Haykin, Editor. Hoboken, NJ, USA: Wiley, 2007.

[5] S. Haykin
Cognitive radar: A way of the future
IEEE Signal Process. Mag., vol. 23, no. 1, pp. 30–40, Jan. 2006.

[6] J. R. Guerci
Cognitive Radio: The Knowledge-Aided Fully Adaptive Approach. Norwood, MA, USA: Artech House, 2010.

[7] H. Deng and B. Himed
Interference mitigation processing for spectrum sharing between radar and wireless communication systems
IEEE Trans. Aerosp. Electron. Syst., vol. 49, no. 3, pp. 1911–1919, Jul. 2013.

[8] H. Griffiths, S. Blunt, L Cohen, and L. Savy
Challenge problems in spectrum engineering and waveform diversity
In *Proc. IEEE Radar Conf.*, Ottawa, ON, Canada, Apr./May 2013, pp. 1–5.

[9] L. K. Patton and B. D. Rigling
Autocorrelation constraints in radar waveform optimization for detection
IEEE Trans. Aerosp. Electron. Syst., vol. 48, no. 2, pp. 951–968, Apr. 2012.

[10] L. K. Patton and B. D. Rigling
Phase retrieval for radar waveform optimization
IEEE Trans. Aerosp. Electron. Syst., vol. 48, no. 4, pp. 3287–3302, Oct. 2012.

[11] L. K. Patton and B. D. Rigling
Autocorrelation and modulus constraints in radar waveform optimization
In *Proc. Int. Waveform Diversity Des. Conf.*, Kissimmee, FL, USA, Feb. 2009, pp. 150–154.

[12] J. Jakabosky, L. Ryan, and S. Blunt
Transmitter-in-the-loop optimization of distorted OFDM radar emissions
In *Proc. IEEE Radar Conf.*, Ottawa, ON, Canada, Apr./May 2013, pp. 1–5.

[13] L. Ryan, J. Jakabosky, S. D. Blunt, C. Allen, and L. Cohen
Optimizing polyphase-coded FM waveforms within a LINC transmit architecture
In *Proc. IEEE Radar Conf.*, Cincinnati, OH, USA, May 2014, pp. 835–839.

[14] S. D. Blunt, J. Jakabosky, M. Cook, J. Stiles, S. Sequin, and E. L. Mokole
Polyphase-coded FM (PCFM) radar waveforms, Part II: Optimization
IEEE Trans. Aerosp. Electron. Syst., vol. 50, no. 3, pp. 2230–2241, Jul. 2014.

[15] N. Kingsley and J. R. Guerci
Adaptive amplifier module technique to support cognitive RF architectures
In *Proc. IEEE Radar Conf.*, Cincinnati, OH, USA, May 2014, pp. 1329–1332.

[16] J.-S. Fu and A. Mortazawi
Improving power amplifier efficiency and linearity using a dynamically controlled tunable matching network
IEEE Trans. Microw. Theory Techn., vol. 56, no. 12, pp. 3239–3244, Dec. 2008.

[17] J. Martin, C. Baylis, L. Cohen, J. de Graaf, and R. J. Marks II
A peak-search algorithm for load-pull optimization of power-added efficiency and adjacent-channel power ratio
IEEE Trans. Microw. Theory Techn., vol. 62, no. 8, pp. 1772–1783, Aug. 2014.

[18] M. Fellows, C. Baylis, J. Martin, L. Cohen, and R. J. Marks II
Direct algorithm for the pareto load-pull optimisation of power-added efficiency and adjacent-channel power ratio
IET Radar, Sonar Navig., vol. 8, no. 9, pp. 1280–1287, Dec. 2014.

[19] J. Sevic, K. Burger, and M. Steer
A novel envelope-termination load-pull method for ACPR optimization of RF/microwave power amplifiers
In *Proc. IEEE MTT-S Int. Microw. Symp. Digest*, Jun. 1998, vol. 2, pp. 723–726.

[20] M. Fellows, C. Baylis, L. Cohen, and R. J. Marks II
Real-time load impedance optimization for radar spectral mask compliance and power efficiency
IEEE Trans. Aerosp. Electron. Syst., vol. 51, no. 1, pp. 591–599, Jan. 2015.

[21] M. Fellows *et al.*
Optimization of power amplifier load impedance and chirp waveform bandwidth for real-time reconfigurable radar
IEEE Trans. Aerosp. Electron. Syst., vol. 51, no. 3, pp. 1961–1971, Jul. 2015.

[22] J. Barkate *et al.*
Fast, simultaneous optimization of power amplifier input power and load impedance for power-added efficiency and adjacent-channel power ratio using the power Smith tube
IEEE Trans. Aerosp. Electron. Syst., vol. 52, no. 2, pp. 928–937, Apr. 2016.

[23] M. Fellows, L. Lamers, C. Baylis, L. Cohen, and R. J. Marks II
A fast load-pull optimization for power-added efficiency under output power and ACPR constraints
IEEE Trans. Aerosp. Electron. Syst., vol. 52, no. 6, pp. 2906–2916, Dec. 2016.

[24] J. Cha, Y. Yang, B. Shin, and B. Kim
An adaptive bias controlled power amplifier with a load-modulated combining scheme for high efficiency and linearity
In *Proc. IEEE Microw. Theory Techn. Soc. Int. Microw. Symp. Digest*, Philadelphia, PA, USA, Jun. 2003, pp. 81–84.

[25] G. Hau, T. B. Nishimura, and N. Iwata
A highly efficient linearized wide-band CDMA handset power amplifier based on predistortion under various bias conditions
IEEE Trans. Microw. Theory Techn., vol. 49, no. 6, pp. 1194–1201, Jun. 2001.

[26] S. Forestier, P. Bouysse, R. Quere, A. Mallet, J.-M. Nebus, and L. Lapierre
Joint optimization of the power-added efficiency and the error-vector measurement of 20-GHz pHEMT amplifier through a new dynamic bias-control method
IEEE Trans. Microw. Theory Techn., vol. 52, no. 4, pp. 1132–1141, Apr. 2004.

[27] M. D. Weiss, F. H. Raab, and Z. Popovic
Linearity of X-band class-F power amplifiers in high-efficiency transmitters
IEEE Trans. Microw. Theory Techn., vol. 49, no. 6, pp. 1174–1179, Jun. 2001.

[28] M. Ranjan, K. H. Koo, G. Harrington, C. Fallesen, and P. Asbeck
Microwave power amplifiers with digitally-controlled power supply voltage for high efficiency and high linearity
In *Proc. IEEE MTT-S Int. Microw. Symp. Digest*, Boston, MA, USA, Jun. 2000, vol. 1, pp. 493–496.

[29] P. Asbeck, L. E. Larson, and I. G. Galton
Synergistic design of DSP and power amplifiers for wireless communications
IEEE Trans. Microw. Theory Techn., vol. 49, no. 11, pp. 2163–2169, Nov. 2001.

[30] F. H. Raab
High-efficiency linear amplification by dynamic load modulation
In *Proc. IEEE MTT-S Int. Microw. Symp. Digest*, Philadelphia, PA, USA, Jun. 2003, vol. 3, pp. 1717–1720.

[31] Y. Yang, K. Choi, and K. P. Weller
DC boosting effect of active bias circuits and its optimization for class-AB InGaP-GaAs HBT power amplifiers
IEEE Trans. Microw. Theory Techn., vol. 52, no. 5, pp. 1455–1463, May 2004.

[32] Y. Yang, J. Yi, Y. Y. Woo, and B. Kim
Optimum design for linearity and efficiency of a microwave Doherty amplifier using a new load matching technique
Microw. J., vol. 44, no. 12, pp. 20–36, 2001.

[33] M. Fellows *et al.*
The bias Smith tube: Simultaneous optimization of bias voltage and load impedance in power amplifier design
In *Proc. IEEE Radio Wireless Symp.*, Austin, TX, USA, Jan. 2016, pp. 215–218.

[34] Y. Sun
Evolutionary tuning method for automatic impedance matching in communication systems
In *Proc. IEEE Int. Conf. Electron., Circuits Syst.*, 1998, vol. 3, pp. 73–77.

[35] Y. Sun and W. K. Lau
Antenna impedance matching using genetic algorithms
In *Proc. IEE Nat. Conf. Antennas Propag.*, York, U.K., Aug. 1999, pp. 31–36.

[36] D. Qiao, R. Molfino, S. Lardizabal, B. Pillans, P. Asbeck, and G. Jerinic
An intelligently controlled RF power amplifier with a reconfigurable MEMS-varactor tuner
IEEE Trans. Microw. Theory Techn., vol. 53, no. 3, pp. 1089–1095, Mar. 2005.

[37] W. du Plessis and P. Abrie
Lumped impedance matching using a hybrid genetic algorithm
Microw. Opt. Technol. Lett., vol. 37, no. 3, pp. 201–212, May 2003.

[38] S. Balachandran and F. C. Y. Lee
Algorithms for power converter design optimization
IEEE Trans. Aerosp. Electron. Syst., vol. 17, no. 3, pp. 422–432, May 1981.

[39] H. C. Calpine and A. Golding
Some properties of pareto-optimal choices in decision problems
Omega, vol. 4, no. 2, pp. 141–147, 1976.

[40] T. Getachew, M. Kostreva, and L. Lancaster
A generalization of dynamic programming for pareto optimization in dynamic networks
RAIRO-Oper. Res., vol. 34, no. 1, pp. 27–47, 2000.

[41] R. T. Marler and J. S. Arora
Survey of multi-objective optimization methods for engineering
Struct. Multidiscip. Optim., vol. 26, no. 6, pp. 369–395, 2004.

[42] K. Deb
Multi-objective optimization
In *Search Methodologies*. New York, NY, USA: Springer, 2005, pp. 273–316.

[43] I. Das and J. E. Dennis
Normal-boundary intersection: A new method for generating the pareto surface in nonlinear multicriteria optimization problems
SIAM J. Optim., vol. 8, pp. 631–657, Mar. 1998.

[44] I. Y. Kim and O. de Weck
Adaptive weighted sum method for multiobjective optimization: A new method for pareto front generation
Struct. Multidiscip. Optim., vol. 31, pp. 105–116, 2006.